

A ^{29}Si MAS NMR and IR spectroscopic investigation of synthetic pyrope-grossular garnet solid solutions

ANNE BOSENICK, CHARLES A. GEIGER

Mineralogisch-Petrographisches Institut, Christian-Albrechts-Universität zu Kiel, Olshausenstrasse 40, D-24098 Kiel, Germany

TORSTEN SCHALLER, ANGELIKA SEBALD

Bayerisches Geoinstitut, Universität Bayreuth, D-95440 Bayreuth, Germany

ABSTRACT

The ^{29}Si MAS NMR spectra of nine pyrope-grossular garnet solid solutions were recorded along with their mid and far infrared spectra. The ^{29}Si MAS NMR spectra of pyrope and grossular measured previously show one single resonance at -72.0 and -83.9 ppm, respectively. A maximum of up to 13 resonances were observed in composition $\text{Py}_{50}\text{Gr}_{50}$ indicating that ^{29}Si MAS NMR spectroscopy can record both first and second shell dodecahedral interactions in garnet. Complete resonance assignments were done by qualitative crystal chemical considerations combined with the comparison of fitted peak intensities with the calculated probabilities for the various possible localized chemical environments around the Si tetrahedra. The NMR spectra of garnets with compositions $\text{Py}_{90}\text{Gr}_{10}$, $\text{Py}_{10}\text{Gr}_{90}$, and $\text{Py}_{05}\text{Gr}_{95}$ are consistent with a random distribution of the divalent cations Ca and Mg on the triangular dodecahedral sites. Garnets with compositions between $0.15 \leq X_{\text{Ca}} \leq 0.75$ show evidence for deviations from random mixing. No overt evidence is found to support a model of local cation order in the most pyrope-rich compositions, which had been proposed on the basis of the asymmetric volumes of mixing along the binary. Powder IR spectra show no additional bands in the solid solutions compared to the end-members, and hence all solid solution compositions are consistent with space group $Ia\bar{3}d$.

INTRODUCTION

Most of the rock-forming silicates are solid solutions involving the substitution of different cations in one or several different structural sites. Of the thermodynamic functions, the volumes and enthalpies of mixing have been determined for many binary silicate solid solutions; it is the entropies of mixing, however, that are generally lacking and that prohibit a better description of many systems. The configurational entropy of mixing can be described by

$$S_{\text{conf}} = k \ln \Omega = k \ln \frac{(N_A + N_B)!}{N_A! \cdot N_B!} \quad (1)$$

where k is Boltzmann's constant and Ω is the number of permutations of $N_A + N_B$ atoms on a structural site. In most thermodynamic models S_{conf} is often calculated assuming complete long-range order or disorder. It is unlikely, though, that these two extreme structural states are always the case, especially in natural minerals that have experienced complicated thermal histories. Garnets are a good case in point, as it is assumed that the aluminosilicate garnet solid solutions ($\text{X}_3\text{Al}_2\text{Si}_3\text{O}_{12}$, where $\text{X} = \text{Fe}^{2+}$, Mn^{2+} , Ca, and Mg) have complete random long-range

disorder in space group $Ia\bar{3}d$, as revealed by single crystal X-ray measurements (i.e., Armbruster et al., 1992).

The determination of short-range order is experimentally more difficult to verify and is limited to a small number of techniques. Solid state magic-angle-spinning nuclear-magnetic-resonance spectroscopy (MAS NMR) offers the possibility to determine quantitatively the state of short-range order of a system. We have investigated the solid solution aluminosilicate garnet binary pyrope ($\text{Mg}_3\text{Al}_2\text{Si}_3\text{O}_{12}$)-grossular ($\text{Ca}_3\text{Al}_2\text{Si}_3\text{O}_{12}$) using ^{29}Si MAS NMR and infrared (IR) spectroscopy to understand the crystal chemistry of this garnet series better.

Pyrope-grossular garnets have received intensive crystal chemical, phase equilibria, and thermodynamic study. The thermodynamic mixing properties ΔH_{mix} , ΔS_{mix} , and ΔV_{mix} show relatively large deviations from ideality. Low-temperature heat capacity measurements on synthetic pyrope, grossular, and the solid solution composition $\text{Py}_{60}\text{Gr}_{40}$ showed that there is considerable excess heat capacity for the solid solution in the range 4–115 K (Haselton and Westrum, 1980). The enthalpy of mixing, ΔH_{mix} , of synthetic pyrope-grossular garnets shows an asymmetric positive deviation, with the largest deviations located toward the pyrope end-member (Newton et al., 1977),

TABLE 1. Synthesis conditions

Sample	Intended composition	P (kbar)	T (°C)	t (h)	Synthesis Type
R-63	pyrope	30	1400	1.0	glass
R-80	Py ₉₀ Gr ₁₀	40	1250	20.5	glass
R-83	Py ₉₀ Gr ₁₀	40	1250	18.0	glass
R-76	Py ₉₀ Gr ₁₀	45	1450	1.5	glass
R-91	Py ₉₀ Gr ₁₀	45	1450	1.5	glass
R-201*	Py ₉₅ Gr ₁₅	25	1100	6.0	glass
R-202*	Py ₉₅ Gr ₁₅	25	1100	6.0	glass
R-203*	Py ₉₅ Gr ₁₅	25	1100	6.0	glass
R-102	Py ₇₅ Gr ₂₅	45	1100	24.5	seeded glass
R-107	Py ₆₀ Gr ₄₀	50	1150	20.0	seeded glass
R-109	Py ₅₀ Gr ₅₀	50	1100	**	seeded glass
R-114	Py ₄₀ Gr ₆₀	50	1150	2.0	seeded glass
R-111	Py ₂₅ Gr ₇₅	50	1050	20.5	seeded glass
R-105	Py ₁₀ Gr ₉₀	50	1150	3.5	seeded glass
R-211*	Py ₉₅ Gr ₉₅	20	1050	20.0	glass
R-212*	Py ₉₅ Gr ₉₅	20	1050	19.0	glass
R-213*	Py ₉₅ Gr ₉₅	20	1050	14.0	glass
R-35	grossular	20	1200	40.5	glass

Note: all samples from Bayreuth except those marked with an asterisk, which are from Kiel.

** Experiment interrupted.

whereas the volumes of mixing, ΔV_{mix} , show positive asymmetric deviations maximized toward the grossular end-member (Ganguly et al., 1993).

Newton and Wood (1980) advanced a crystal chemical model (equivalent site behavior) to explain the asymmetry in ΔV_{mix} , whereby a certain degree of cation ordering should exist for compositions near the smaller cation end-member (i.e., pyrope). The substitution of the larger Ca cation into the structure of pyrope is thought to produce localized site deformations and thus high free energy gradients around the substituent, which makes it less probable for other Ca cations to enter the structure in the immediate neighborhood. A preliminary single crystal X-ray study on synthetic garnet of composition Py₉₀Gr₁₀ left open the possibility for a space group lower than $Ia\bar{3}d$ (Dempsey, 1980). If true, the single eight-fold coordinated X site in space group $Ia\bar{3}d$ would degenerate into two or more crystallographically inequivalent sites, where ordering of Ca and Mg cations could take place.

The major goal of this work is, therefore, to determine the structural state of synthetic pyrope-grossular garnets.

EXPERIMENTAL METHODS

Synthesis

Pyrope-grossular garnets were synthesized from glasses and seeded glasses at high pressures and temperatures in a piston-cylinder device at Kiel and Bayreuth (Geiger et al., 1990b). The following oxides were used to prepare the glasses: MgO [Johnson Matthey Alfa Products (JM), 99.999%], CaCO₃ (JM, ultrapure), SiO₂ (JM, 99.999%), and Al₂O₃ (JM, 99.99%). All oxides, except CaCO₃, were heated at 1100–1200 °C for about 1 d, reground and fired at 1200 °C for another 24 h before weighing; CaCO₃ was dried at 300 °C for 48 h prior to weighing. Three grams of oxide mixtures of the appropriate garnet compositions were mixed and ground intimately under distilled water. The oxide mixtures were heated at a rate of 100°/h to 1000 °C and held for 10–12 h to remove CO₂. The decarbonized oxide mixtures were pressed into pellets, melted in a Pt₉₅Au₀₅-crucible for about 30 min, and quenched to glass in a water bath. The glasses were ground in an agate mortar and remelted a second time. The temperatures at which the melts were prepared were: 1450 °C for grossular, 1650 °C for pyrope, and between 1450 and 1650 °C for the intermediate members depending on their composition. The first melting yielded >95% glass with some crystalline material, and the second produced better than 99% glass. Microprobe analysis of the glasses showed them to be homogenous within 1% ($\pm 1\sigma$) of their average composition and closely matching their intended composition.

The synthesis conditions of the pyrope-grossular garnets are summarized in Table 1. All syntheses were done anhydrously. Pt capsules of diameter 4.5 mm and containing 150–200 mg of glass were used in syntheses above 30 kbar, and 5.0 mm diameter capsules containing 200–250 mg of material for the syntheses below 30 kbar were employed. Some compositions, especially the more grossular-rich garnets, required seeding to obtain nearly 100% garnet yields. The garnet seeds were synthesized hydrothermally in Pt capsules using glass and distilled water as a flux. The garnets so produced were relatively coarse-grained but generally more inhomogeneous in composition. They were finely reground and mixed with the start-

TABLE 2. Microprobe analyses of synthetic pyrope-grossular garnets*

Sample	R-80	R-83	R-91	R-201	R-202	R-102	R-107
SiO ₂	44.67(14)	44.73(43)	44.44(27)	43.57(95)	43.63(98)	44.25(53)	43.27(14)
Al ₂ O ₃	25.11(21)	25.06(17)	25.08(17)	24.25(80)	24.38(77)	24.17(47)	23.88(9)
FeO	0.02(2)	0.02(3)	0.04(3)	0.01(1)	0.00(1)	0.03(3)	0.03(2)
CaO	4.18(14)	4.26(9)	4.25(9)	6.28(23)	6.28(24)	10.54(45)	16.39(38)
MgO	26.19(23)	26.26(23)	26.28(18)	23.91(56)	24.03(57)	20.90(26)	16.68(23)
Total	100.16	100.34	100.11	98.02	98.32	99.89	100.24
Si	3.028(4)	3.030(26)	3.016(12)	3.036(66)	3.032(64)	3.064(35)	3.036(4)
Al	2.006(16)	2.002(39)	2.006(10)	1.992(54)	1.996(52)	1.972(36)	1.974(8)
Fe	0.000(1)	0.002(1)	0.002(1)	0.000(1)	0.000(1)	0.002(1)	0.002(1)
Ca	0.304(10)	0.310(6)	0.309(6)	0.470(14)	0.468(16)	0.782(34)	1.232(27)
Mg	2.646(20)	2.650(25)	2.658(16)	2.484(23)	2.488(25)	2.156(25)	1.744(24)
Sum	7.984	7.992	7.991	7.984	7.986	7.976	7.988
mol% Py	89.70(67)	89.56(81)	89.58(54)	84.10(76)	84.17(76)	73.40(83)	58.60(81)
mol% Gr	10.30(34)	10.44(24)	10.42(21)	15.90(48)	15.83(48)	26.60(99)	41.40(91)

* Normalized to 12 O atoms.

ing glasses with the ratio of glass to seed material for the final syntheses being about 6 or 7:1. The solid solution syntheses over 30 kbar were done using a 1/2 in. talc-glass assembly and those under 30 kbar a salt-based assembly. The synthesis experiments were quenched to room temperature by switching off the power. The polycrystalline experimental products constituting nearly 100% garnet were characterized by optical microscopy, electron microprobe, and X-ray diffraction analysis. The garnets were optically isotropic with the size of the crystals generally between 5 and 10 μm .

The garnets were analyzed with a Cameca Camebax microprobe in Kiel and Bayreuth with an accelerating voltage of 15 kV and a beam current of 30 mA using common oxides and silicates as standards. The diameter of the electron beam was approximately 1 μm . Each spot was measured for 20 s and the background for 10 s. The results of the microprobe analyses are given in Table 2. Each analysis represents an average of generally 15–20 random spot measurements. Standard deviations are given in parentheses. All garnets were also characterized using an automated powder X-ray diffractometer (Stoe or Siemens) using $\text{CuK}\alpha$ radiation. The diffraction patterns were recorded from 20 to 130° 2θ using 0.01° 2θ increments. All patterns display resolution of the $K\alpha_1$ – α_2 peaks around 60° 2θ , which has been proposed as a general indicator of homogeneity of garnet solid solutions (Ganguly et al., 1993). All peaks, with exception of a very weak peak indexed to the strongest reflection of quartz, could be indexed to garnet. Results from the powder diffraction analysis including cell-dimension refinements are presented elsewhere (Bosenick and Geiger, in preparation). The preliminary data are in good agreement with the results of Ganguly et al. (1993).

IR spectroscopy

Powder infrared spectra were measured at the Anorganisch-Chemisches Institut der Universität Kiel. They were recorded using a Nicolet 5 DB spectrometer equipped with a KBr beam-splitter in the mid-infrared region (MIR, 400–4000 cm^{-1}) and using a Bruker IFS 66 spectrometer in the far-infrared region (FIR, 530–80 cm^{-1}). Between

0.5 and 1.0 mg of garnet, which was previously finely ground in an agate mortar under distilled water, was used to make pellets pressed under vacuum. Matrix material for the MIR measurements was KBr and, for the FIR spectra polyethylene was used. A total of 128 scans were recorded and averaged for each final spectrum. The resolution adopted was 4 cm^{-1} in the MIR and 2 cm^{-1} in the FIR.

^{29}Si MAS NMR spectroscopy

The 59.6 MHz ^{29}Si MAS NMR spectra were measured using a Bruker MSL 300 NMR spectrometer. The ^{29}Si chemical shifts are reported relative to an external Me_4Si (TMS) standard equal to 0 ppm. The spectra were collected using a 7-mm double-bearing CP/MAS Bruker probe, with pulse durations of 2 μs , corresponding to 36° pulses. Relaxation delays of 30 s were sufficient to allow for complete relaxation; spinning frequencies were between 3.0 and 3.6 kHz. In some cases, the amount of sample (150–300 mg) was insufficient to fill the rotor completely. To avoid mixing the garnets with other materials, these ^{29}Si MAS NMR spectra were collected using an airtight Kel-F rotor insert (ca. 100 mg of sample) designed to fit exactly inside the ZrO_2 rotor (Merwin et al., 1989). The number of scans measured varied between 100 for the end-members (Geiger et al., 1990a) and up to 3000 for $\text{Py}_{50}\text{Gr}_{50}$. To obtain good quality spectra with high signal to noise ratios three different syntheses, made at identical P - T conditions, were combined for solid solution compositions $\text{Py}_{85}\text{Gr}_{15}$ and $\text{Py}_{95}\text{Gr}_{5}$ (Table 1).

Relative peak intensities were obtained by fitting the spectra to a sum of Lorentzian and Gaussian curves using a program written by J. Kümmerlen (Geoinstitut Bayreuth). The program optimizes peak positions, peak shapes, and full width at half maximum (FWHM) for up to 13 individual resonances, and each of the fitting parameters can be separately constrained.

RESULTS

IR spectroscopy

The observed IR spectra are essentially identical (Fig. 1a and 1b) to those recorded previously in an earlier study

TABLE 2.—Continued

Sample	R-109	R-114	R-111	R-105	R-211	R-212	R-213
SiO_2	42.74(19)	41.99(31)	41.17(19)	40.53(19)	40.61(14)	40.70(18)	40.56(21)
Al_2O_3	23.69(19)	23.37(13)	22.99(12)	22.68(10)	22.34(11)	22.44(14)	22.40(14)
FeO	0.02(2)	0.02(2)	0.02(2)	0.01(1)	0.02(2)	0.02(2)	0.03(2)
CaO	20.11(35)	24.01(34)	28.49(36)	34.71(23)	36.98(20)	36.80(19)	36.61(29)
MgO	13.78(24)	10.92(20)	6.67(21)	2.67(15)	1.35(10)	1.36(9)	1.37(10)
Total	100.35	100.30	100.35	100.60	101.30	101.52	100.98
Si	3.028(12)	3.012(15)	3.001(8)	2.994(9)	2.998(4)	3.002(8)	3.002(9)
Al	1.978(13)	1.976(4)	1.975(8)	1.974(8)	1.942(7)	1.950(8)	1.954(7)
Fe	0.002(1)	0.002(1)	0.001(1)	0.002(1)	0.002(1)	0.002(2)	0.002(2)
Ca	1.528(27)	1.846(28)	2.303(30)	2.747(18)	2.924(13)	2.908(14)	2.902(15)
Mg	1.456(24)	1.168(19)	0.725(22)	0.293(16)	0.148(11)	0.150(10)	0.150(11)
Sum	7.992	8.002	8.006	8.009	8.016	8.012	8.010
mol% Py	48.80(79)	38.75(63)	23.94(73)	9.64(52)	4.82(36)	4.88(35)	4.93(35)
mol% Gr	51.20(91)	61.25(92)	76.06(98)	90.36(59)	95.18(43)	95.12(43)	95.07(51)

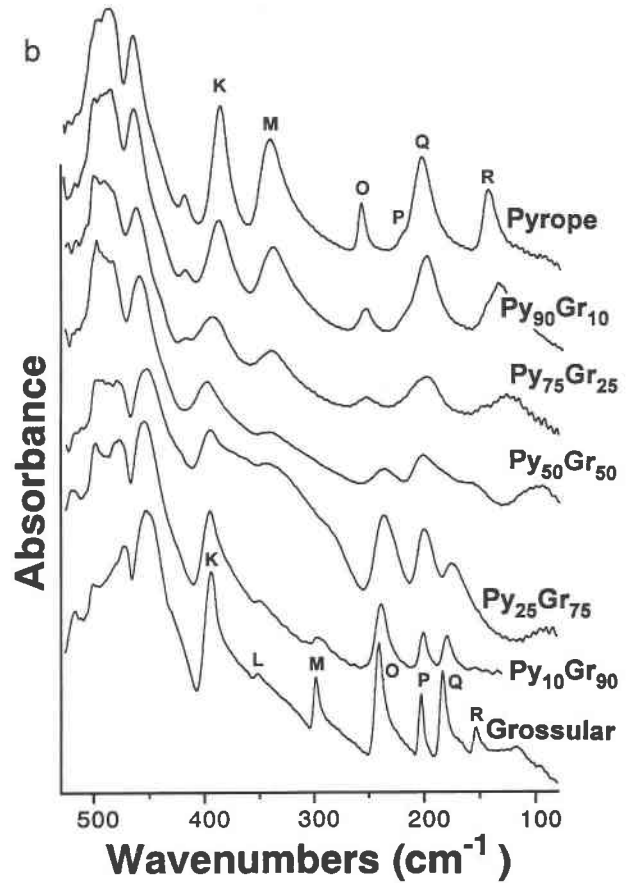
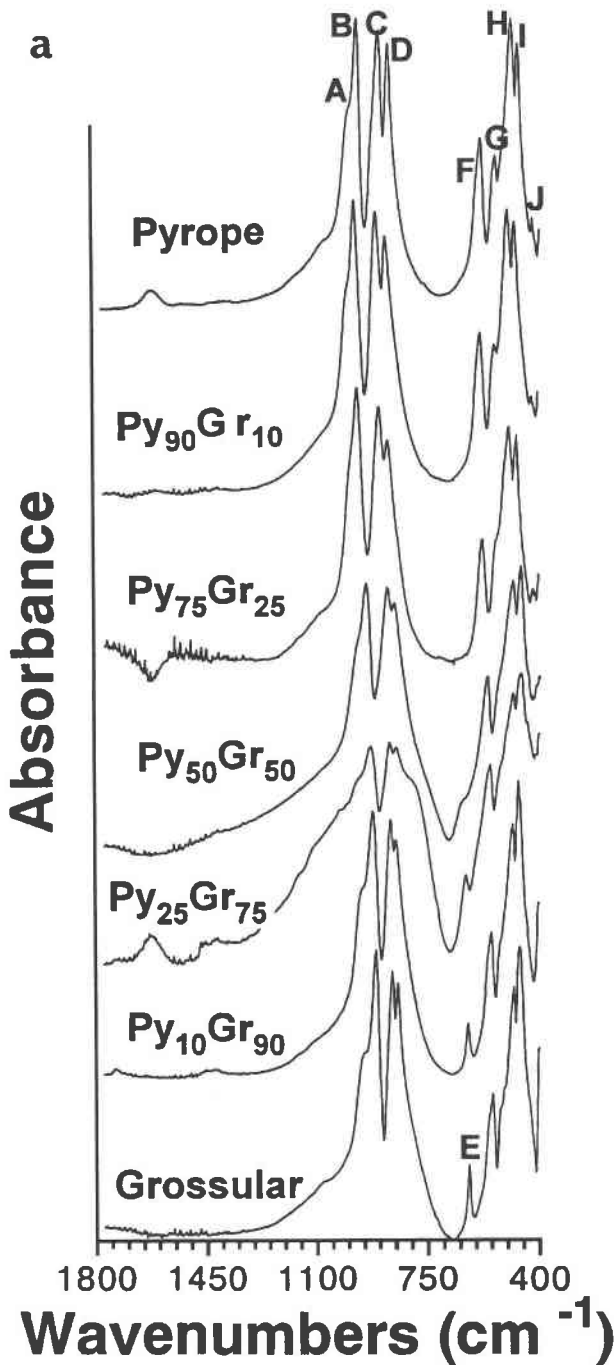


Fig. 1. (a) MIR spectra of pyrope-grossular garnets from 1800 to 400 cm^{-1} . (b) FIR spectra of pyrope-grossular garnets from 530 to 125 cm^{-1} .

of pyrope-grossular solid solutions (Delany, 1981). Garnet compositions with $0.40 \leq X_{\text{Ca}} \leq 0.96$ could not be synthesized by Delany (1981) but were achieved in this study (Geiger et al., 1990b). Our spectra generally show better resolution in the far-infrared region. The IR bands have been labeled alphabetically following Tarte (1965) and have no physical significance. The band positions (Table 3) and their shifts as a function of composition are shown in Figure 2.

^{29}Si MAS NMR spectroscopy

The ^{29}Si MAS NMR spectra of synthetic end-member pyrope and grossular are characterized by a single resonance with chemical shifts of -72.0 and -83.9 ppm, respectively (Geiger et al., 1990a, 1992). The ^{29}Si MAS NMR spectra of the pyrope-rich solid solution compositions $\text{Py}_{90}\text{Gr}_{10}$, $\text{Py}_{85}\text{Gr}_{15}$, and $\text{Py}_{75}\text{Gr}_{25}$ show good peak resolution (Fig. 3a). In the spectrum of $\text{Py}_{90}\text{Gr}_{10}$ five res-

onances are observable with chemical shifts at -72.3 , -73.4 , -74.6 , -75.5 , and -76.7 ppm, where the error in the peak positions is about ± 0.2 ppm. The resonance at -72.3 ppm has the largest intensity and has the same chemical shift as the single resonance observed in pyrope. These same five resonances are also observed in the spectra of $\text{Py}_{85}\text{Gr}_{15}$ and $\text{Py}_{75}\text{Gr}_{25}$, with the addition of a weak resonance at -77.8 ppm in $\text{Py}_{85}\text{Gr}_{15}$ and in $\text{Py}_{75}\text{Gr}_{25}$ a seventh possible resonance at -78.8 ppm. The relative peak intensities of the first five resonances change markedly in $\text{Py}_{75}\text{Gr}_{25}$ compared to those in $\text{Py}_{90}\text{Gr}_{10}$ and $\text{Py}_{85}\text{Gr}_{15}$, but the resonance at -72.3 ppm still shows the greatest intensity. In the spectrum of $\text{Py}_{75}\text{Gr}_{25}$ the peak at -73.4 ppm approaches the intensity of the -72.3 ppm resonance, whereas it had only about a half or a third the intensity in the other two compositions.

The ^{29}Si MAS NMR spectra of the grossular-rich solid solutions $\text{Py}_{05}\text{Gr}_{95}$, $\text{Py}_{10}\text{Gr}_{90}$, and $\text{Py}_{25}\text{Gr}_{75}$ show two broad resonance envelopes centered around -83.7 and -80.1 ppm (Fig. 3b). In the spectrum of $\text{Py}_{05}\text{Gr}_{95}$, the resonance at -83.7 ppm has about ten times the intensity of the resonance at -80.1 ppm and displays a small shoulder around -83.1 ppm. In the spectrum of $\text{Py}_{10}\text{Gr}_{90}$ this shoulder becomes more pronounced and a second shoulder located at about -82.5 ppm also appears. The intensity of the resonance at -80.1 ppm is about one fourth of the resonance at -83.8 ppm and displays a possible additional shoulder around -79.3 ppm. In the spectrum of $\text{Py}_{25}\text{Gr}_{75}$ the two broad envelopes at about -80.1 and -83.7 ppm have nearly similar intensities. Additional shoulders at about -78.2 , -77.4 ppm, and around -81.3 ppm are observable.

The ^{29}Si MAS NMR spectra of the solid solutions of intermediate compositions $\text{Py}_{60}\text{Gr}_{40}$, $\text{Py}_{50}\text{Gr}_{50}$, and $\text{Py}_{40}\text{Gr}_{60}$ show slightly poorer signal to noise ratios (Fig. 3c). For these three spectra, the resonances between -76.5

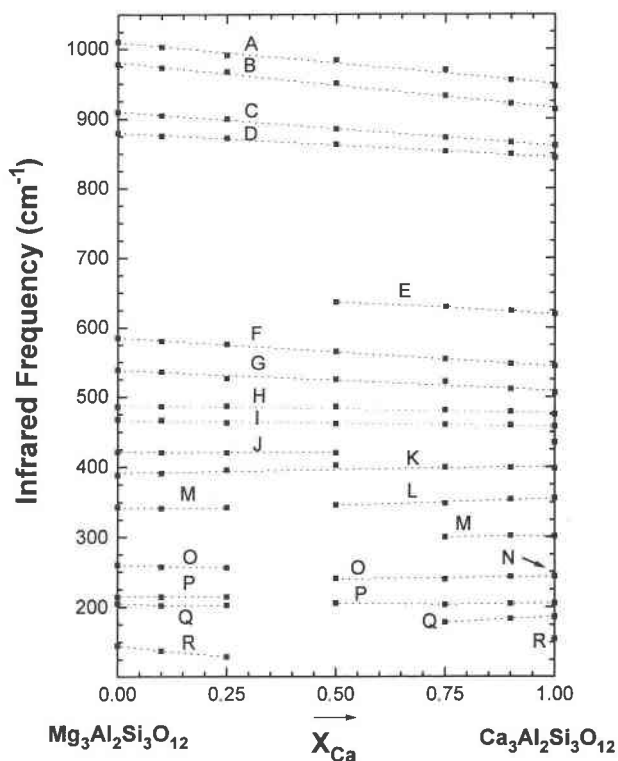


Fig. 2. Plot of the IR bands in wavenumbers vs. garnet composition.

$\geq \delta \geq -80.1$ ppm have the greatest intensities. In the spectrum of $\text{Py}_{40}\text{Gr}_{60}$, in addition to the two broad resonance envelopes centered at -83.8 and -80.1 ppm and present in the grossular-rich spectra, low intensity reso-

TABLE 3. Positions of the IR bands of synthetic pyrope-grossular garnets

IR band	Pyrope	$\text{Py}_{90}\text{Gr}_{10}$	$\text{Py}_{75}\text{Gr}_{25}$	$\text{Py}_{60}\text{Gr}_{50}$	$\text{Py}_{25}\text{Gr}_{75}$	$\text{Py}_{10}\text{Gr}_{90}$	Grossular
MIR band positions (cm^{-1})							
A	1010 sh	1002 sh	991 sh	984 sh	970 sh	955 sh	946 sh
B	978 vs	972 vs	967 vs	951 vs	933 s	921 vs	913 vs
C	909 vs	904 vs	899 vs	885 vs	873 s	866 vs	861 vs
D	879 vs	875 vs	872 vs	863 vs	853 s	848 vs	843 vs
E	—	—	—	637 sh	629 m	623 m	619 m
F	584 s	580 s	575 s	565 s	554 s	547 s	543 s
G	538 m	535 m	526 sh	525 sh	521 sh	511 sh	505 sh
H	486 vs	486 vs	486 vs	485 vs	481 vs	478 vs	475 vs
I	467 vs	466 vs	462 vs	461 vs	460 vs	459 vs	458 vs
J	421 mw	420 mw	420 mw	420 w	—	—	—
FIR band position (cm^{-1})							
K	388 m	390 m	395 vs	402 m	399 m	399 m	398 m
L	—	—	—	345 w	348 mw	354 w	355 w
M	342 m	341 m	342 mw	—	300 sh	301 w	301 mw
N	—	—	—	—	—	—	243 d
O	259 mw	256 w	255 w	240 mw	239 m	243 mw	243 m
P	214 sh	214 sh	214 sh	205 mw	203 m	204 mw	205 m
Q	204 m	201 m	202 mw	—	178 mw	183 mw	186 m
R	144 m	137 mw	129 w	—	—	—	155 mw

Note: intensity indication: sh = shoulder, vs = very strong, s = strong, m = medium, mw = medium to weak, w = weak, d = doublet.

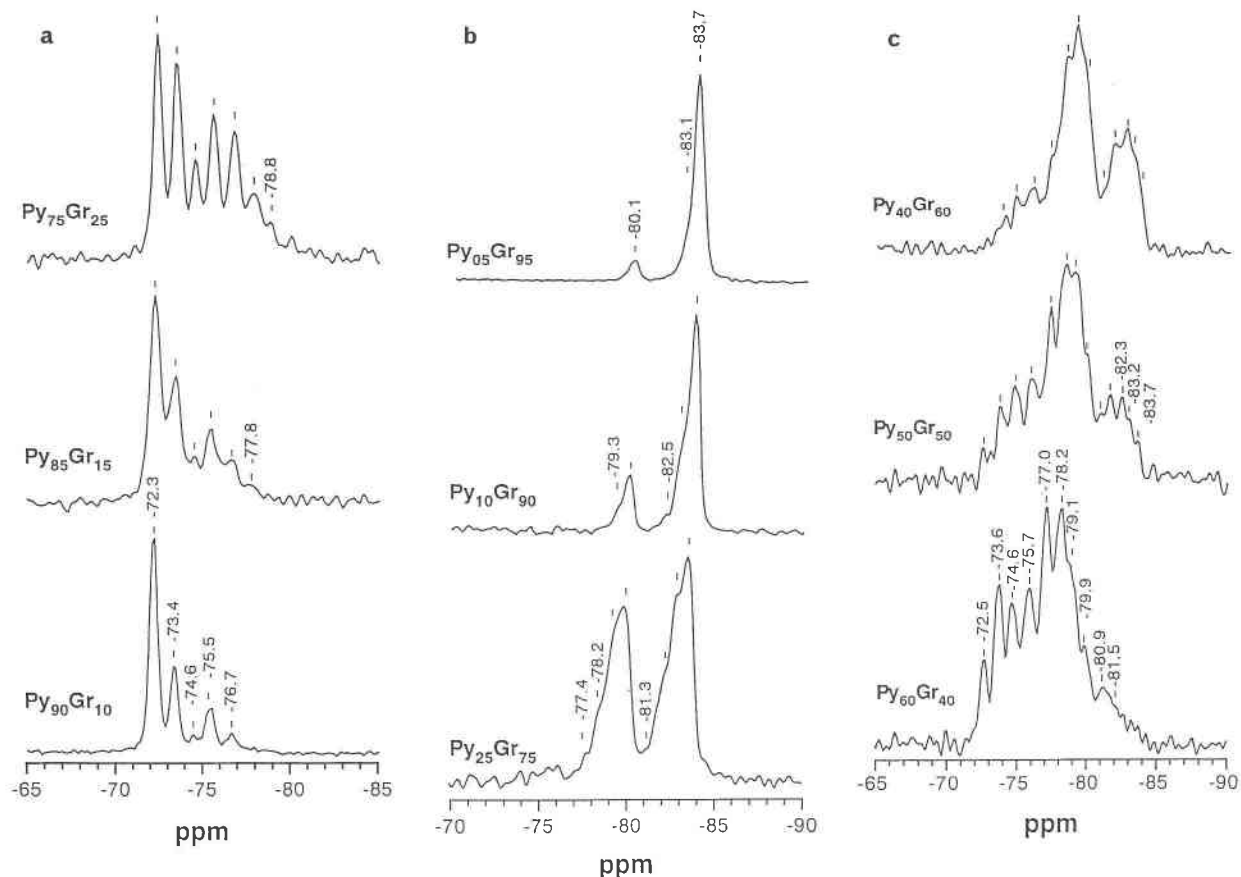


Fig. 3. (a) The 59.6 MHz ^{29}Si MAS NMR spectra of pyrope-rich garnets $\text{Py}_{90}\text{Gr}_{10}$, $\text{Py}_{85}\text{Gr}_{15}$, and $\text{Py}_{75}\text{Gr}_{25}$. (b) The 59.6 MHz ^{29}Si MAS NMR spectra of grossular-rich garnets $\text{Py}_{05}\text{Gr}_{95}$, $\text{Py}_{10}\text{Gr}_{90}$, and $\text{Py}_{25}\text{Gr}_{75}$. (c) The 59.6 MHz ^{29}Si MAS NMR spectra of intermediate composition garnets $\text{Py}_{40}\text{Gr}_{60}$, $\text{Py}_{50}\text{Gr}_{50}$, and $\text{Py}_{60}\text{Gr}_{40}$.

nances located between $-72.0 \geq \delta \geq -77.7$ ppm are observed. In the spectrum of $\text{Py}_{50}\text{Gr}_{50}$ the resolution is better, and up to 13 individual resonances can be observed. In $\text{Py}_{60}\text{Gr}_{40}$ the same chemical shift resonances as in the spectrum of $\text{Py}_{75}\text{Gr}_{25}$ are present in addition to weaker resonances at $\delta \leq -78.8$ ppm.

DISCUSSION

IR spectroscopy

The energies of the MIR bands change essentially linearly with composition, and no clear relation between the degree of band shifts and the volumes of mixing was observed, as reported for almandine-grossular solid solutions (Geiger et al., 1989). The line widths in the spectra of the solid solutions are broader than those of the end-members. Line broadening is generally associated with cation disorder and indicates, qualitatively at least, the absence of significant long-range order of Mg and Ca in the dodecahedral sites. Theoretical factor group analysis of garnet of space group $Ia\bar{3}d$ predicts that there should be a total of 17 active IR bands (Moore et al., 1971).

Space groups of lower symmetry should increase the number of active bands. For example, a change to space group $I2_13$, as suggested by Dempsey (1980) for a garnet of composition $\text{Py}_{90}\text{Gr}_{10}$, should result in 58 active IR bands being present (Delany, 1981). The powder IR spectrum of pyrope shows 14 IR bands and that of grossular 16 IR bands (Fig. 1a and 1b). The IR spectra of the solid solution garnets show no more than 17 bands, and hence there is no overt indication for symmetry lowering.

Band assignments for the garnets could be made consistently with those proposed from the single-crystal IR spectra of natural garnets (Hofmeister and Chopelas, 1991). Band positions are within 2 cm^{-1} for the TO positions given by Hofmeister and Chopelas (1991), except for bands I and J, which differ by 10 and 5 cm^{-1} , respectively. The energy differences or splitting between the TO and LO modes are only strongly developed in the mid-infrared region. The origin of band A is not clear (McMillan et al., 1989). Bands B, C, and D belong to the asymmetric Si-O stretching mode, ν_3 , of the SiO_4 groups. Bands E, F, and G are assigned to the symmetric bending mode, ν_4 , and band I to the asymmetric bending mode,

ν_2 , of the SiO_4 tetrahedra. Bands K and L have been assigned to tetrahedral rotations, $R(\text{SiO}_4)$, and band M to a translation, $T(\text{SiO}_4)$, of the SiO_4 tetrahedra. Band R is thought to be a mixture of SiO_4 and other cation translations, $T(\text{SiO}_4)_{\text{mix}}$. Bands H, J, and N are assigned to translations of the Al octahedra, $T(\text{Al})$ and bands O, P, and Q to translations of the X cations, $T(\text{X})$, in the dodecahedral site (Hofmeister and Chopelas, 1991).

Hofmeister and Chopelas (1991) proposed that in the spectrum of grossular two overlapping bands are present around 244 cm^{-1} . The band at 243 cm^{-1} in our spectrum is asymmetric. No splitting or noticeable doubling is observed. In the case of pyrope, Hofmeister and Chopelas (1991) observed all 17 IR active bands. In our powder spectrum the bands labeled E, M, and N could not be identified.

The assignment of the bands for the solid solution garnets was made by following their shifts as a function of composition. The band assignments in the FIR region cannot be made with complete certainty in the middle part of the binary because of significant band broadening. Band assignments in the FIR region were interpreted using the model of two-mode behavior as described by Hofmeister and Chopelas (1991). Two-mode behavior predicts that the compositions located near the two end-members are characterized by vibrations similar in energy to those of the end-member. Simple linear interpolation of the modes between pyrope and grossular cannot be made. In the case of the pyrope-grossular binary, the $T[\text{X}]$ and $T[\text{SiO}_4]$ vibrations are characterized by two-mode behavior. Two-mode behavior results from differences in size and/or mass of the X-site cations. It is also present, however, in $T[\text{SiO}_4]$ vibrations because of the edge-sharing relationship between tetrahedra and dodecahedra (Hofmeister and Chopelas, 1991).

The IR spectra also permit some crystal chemical interpretations. Moore et al. (1971) suggested that the degree of separation of bands C and D, defined as site group splitting, is a measure of SiO_4 tetrahedral distortion. The site group splitting is 30 and 18 cm^{-1} in pyrope and grossular, respectively, and changes linearly as a function of composition across the join (Fig. 4a). Tetrahedral distortion derived from diffraction experiments has also been calculated (Renner and Lehmann, 1986), using X-ray powder Rietveld refinement data from Ganguly et al. (1993) and can be compared to the IR data. Tetrahedral distortion is greatest for pyrope (Fig. 4b). The edge-length distortion index decreases linearly with increasing grossular content, as does the angular distortion of the SiO_4 tetrahedra within the limits of the data. Moore et al. (1971) also proposed the term factor group splitting, which is defined as the ratio of $[B - (C + D)/2]$. It is proposed to be a measure of the degree of vibrational interaction between the isolated SiO_4 groups and increases with decreasing distance between the SiO_4 tetrahedra. The factor group splitting is larger than the site group splitting and decreases with increasing grossular content from 84 cm^{-1} in pyrope to 61 cm^{-1} in grossular and does not follow a

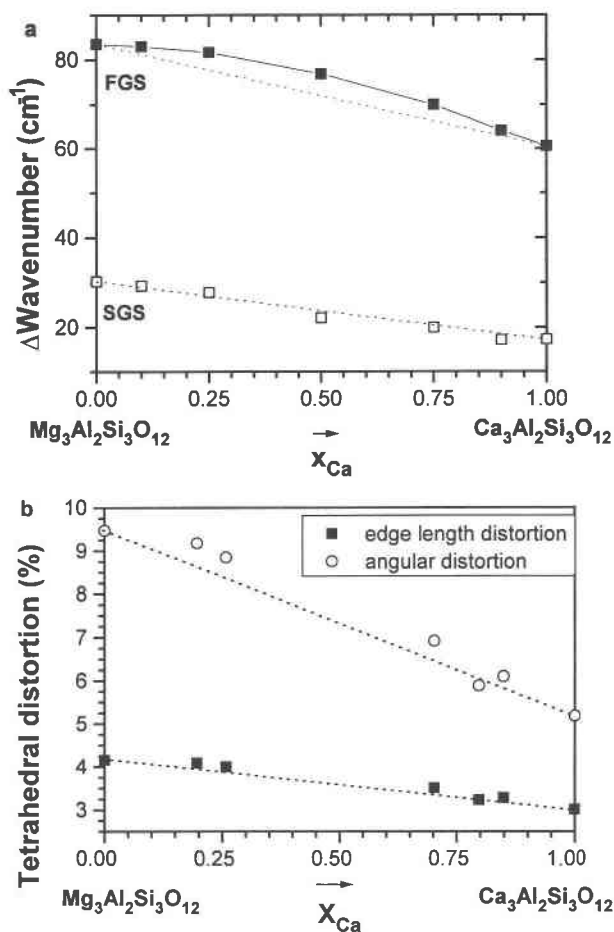


Fig. 4. (a) Variation of factor group splitting [$\text{FGS} = B - (C + D)/2$] and site group splitting ($\text{SGS} = C - D$) as a function of garnet composition. (b) Edge length and angular tetrahedral distortion (Renner and Lehmann, 1986) plotted as a function of composition. The structural data were taken from Ganguly et al. (1993).

linear trend between the two end-members (Fig. 4a). It remains nearly constant from pyrope to $\text{Py}_{75}\text{Gr}_{25}$ and then decreases with increasing grossular content.

^{29}Si MAS NMR spectroscopy

The ^{29}Si MAS NMR spectroscopy is sensitive to the chemical and structural environment around the ^{29}Si nuclei. Changes in the chemical environment (e.g., dodecahedral sites in garnet) can induce changes in the chemical shift, where each individual resonance reflects a unique chemical or structural environment sensed by the Si nuclei. Moreover, single pulse ^{29}Si MAS NMR is quantitative, provided sufficiently long relaxation delays and/or small pulse angles are used in conjunction with MAS rates suitable to average all anisotropic ^{29}Si shielding contributions. Therefore, the relative intensities of the different isotropic ^{29}Si resonances indicate the number of Si nuclei residing within a unique structural environment.

Pyrope-grossular solid solutions, $(\text{Mg}_x\text{Ca}_{1-x})_3\text{Al}_2\text{Si}_3\text{O}_{12}$, can

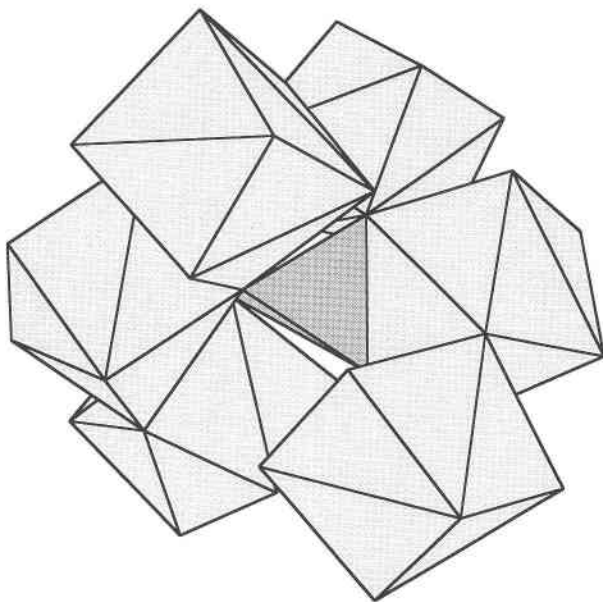


Fig. 5. Diagram showing the local dodecahedral configuration surrounding an isolated Si tetrahedron in the garnet structure. The two edge-shared dodecahedra form a first or inner coordination shell and the four corner-shared dodecahedra form a second or outer coordination shell.

be described by an exchange of Ca and Mg on the dodecahedral site, whereas all of the octahedra are occupied by Al. Garnets of space group $Ia\bar{3}d$ contain a single crystallographically independent Si site (Menzer, 1928), where each Si tetrahedra shares two edges and four corners with differing and neighboring dodecahedra (Fig. 5). The Si-X1 distance, where X = Ca or Mg, for the two edge-shared dodecahedra, is 2.86 Å in pyrope and 2.96 Å in grossular (Novak and Gibbs, 1971). The Si-X2 distance of the four-corner shared dodecahedra is 3.51 Å and 3.63 Å in pyrope and grossular, respectively. The edge-shared dodecahedra form an inner or first coordination shell around a given Si tetrahedron, and the corner-shared dodecahedral sites form an outer or second coordination shell (Fig. 5). There are three possible and unique cation configurations for the two edge-shared dodecahedra in the first shell, that is Mg-Si-Mg, Mg-Si-Ca, and Ca-Si-Ca. For the second shell there are five possible configurations, given as MgMgMgMg, MgMgMgCa, MgMgCaCa, MgCaCaCa, and CaCaCaCa for the four corner-shared dodecahedra. Hence, there are $3 \times 5 = 15$ unique and possible local arrangements or configurations around a Si site. The exchange of different sized divalent cations in the dodecahedral sites causes changes in bond lengths and angles such as Si-Al distances, tetrahedral-octahedral Si-O-Al angles, etc. Variations of these quantities could therefore be responsible to a certain degree for the observed changes in the chemical shifts. However, they are considered to be secondary in importance, as the driving forces for these variations is the substitution of Mg for Ca in the dodecahedral sites.

In pyrope, all dodecahedra are occupied with Mg cations and in grossular by Ca cations. Both spectra display a single resonance, in pyrope at -72.0 ppm corresponding to the two shell configuration MgMg-MgMgMgMg and in grossular at -83.9 ppm corresponding to CaCa-CaCaCaCa (Geiger et al., 1990a, 1992). The Si chemical shifts become more shielded (i.e., more negative) with the substitution of Ca for Mg cations. In both end-members only a single Si-site geometry is present locally, as in the average long-range structure. As there is no indication of a space group lower than $Ia\bar{3}d$ in the solid solutions, any additional resonances that would be observable in the ^{29}Si MAS NMR spectra would have to be caused by different nearest dodecahedral or next-nearest dodecahedral interactions (i.e., configurations), rather than from the presence of crystallographically independent Si sites occurring in a lower space group symmetry. In the case that the NMR measurements were only sensitive to the first shell interactions with Mg and Ca in edge-shared dodecahedra, the spectra of the solid solutions would show no more than three resonances: one resonance at approximately -72.0 ppm corresponding to Mg-Si-Mg as observed in pyrope, one resonance at approximately -83.9 ppm corresponding to Ca-Si-Ca as in grossular, and one resonance between $-72.0 \geq \delta \geq -83.9$ ppm corresponding to the mixed arrangement Mg-Si-Ca.

Resonance assignments of the solid solution garnets

The spectrum of $\text{Py}_{90}\text{Gr}_{10}$ displays five resonances (Fig. 3a) and the other solid solution compositions even more, indicating that ^{29}Si MAS NMR spectroscopy is sensitive to first and second shell interactions in garnet. This is, to the best of our knowledge, the first time that two interaction shells have been observed using ^{29}Si MAS NMR spectroscopy. In $\text{Py}_{90}\text{Gr}_{10}$ the peak at -72.3 ppm is identical to the resonance observed in pyrope and thus is readily assigned to the configuration MgMg-MgMgMgMg. The amount of shielding of an atom is inversely proportional to its distance to the Si atom (Engelhardt and Michel, 1987), and therefore, the substitution of Ca for Mg in the first shell results in a larger change of the chemical shift than the same substitution in the second shell. The smallest change toward a more negative chemical shift value (i.e., greater shielding) should be due to the substitution of one Ca for one Mg in the second shell. The resonance at -73.4 ppm is thus assigned to MgMg-MgMgMgCa (Fig. 3a). The other resonances at -74.6 , -75.5 , and -76.6 ppm cannot, however, be assigned similarly by such qualitative considerations, because one cannot predict, or calculate from first principles, whether the substitution of one Ca for one Mg cation in the first shell results in a greater or smaller change of the chemical shift than the substitution of two Ca cations for two Mg cations in the second shell.

In the NMR spectrum of $\text{Py}_{05}\text{Gr}_{95}$ the strong resonance at -83.7 ppm is identical with the resonance observed in grossular and is assigned to CaCa-CaCaCaCa (Fig. 3b). The shoulder at -83.1 ppm is assigned to the configu-

TABLE 4. General formulae for calculating statistical probabilities in a random model for the 15 different configurations around the Si cations

Second shell	First shell		
	MgMg	MgCa	CaCa
MgMgMgMg	$(1 - X_{Ca})^8$	$2(1 - X_{Ca})^5 X_{Ca}$	$(1 - X_{Ca})^4 X_{Ca}^4$
MgMgMgCa	$4(1 - X_{Ca})^5 X_{Ca}$	$8(1 - X_{Ca})^4 X_{Ca}^2$	$4(1 - X_{Ca})^3 X_{Ca}^3$
MgMgCaCa	$6(1 - X_{Ca})^4 X_{Ca}^2$	$12(1 - X_{Ca})^3 X_{Ca}^3$	$6(1 - X_{Ca})^2 X_{Ca}^4$
MgCaCaCa	$4(1 - X_{Ca})^3 X_{Ca}^3$	$8(1 - X_{Ca})^2 X_{Ca}^4$	$4(1 - X_{Ca}) X_{Ca}^5$
CaCaCaCa	$(1 - X_{Ca})^2 X_{Ca}^6$	$2(1 - X_{Ca}) X_{Ca}^5$	X_{Ca}^6

ration CaCa-MgCaCaCa, because it has the smallest change in the chemical shift toward less negative values. The grossular-rich spectra by $Py_{0.5}Gr_{9.5}$, $Py_{10}Gr_{90}$, and $Py_{25}Gr_{75}$ show two broad resonance envelopes as one would expect for first shell interactions only (Fig. 3b). Therefore, we assume that the broad resonance envelope around -83.8 ppm contains several overlapping resonances, where only Ca cations are present in the first shell (i.e., CaCa-XXXX), whereas the envelope centered at about -80.1 ppm corresponds to all those configurations where one Ca and one Mg is present in the first shell (i.e., CaMg-XXXX). The individual resonances can then be assigned as following: CaCa-MgMgCaCa at -82.5 ppm, CaCa-MgMgMgCa at -81.3 ppm, MgCa-CaCaCaCa at -80.1 ppm, MgCa-MgCaCaCa at -79.3 ppm, and MgCa-MgMgCaCa at -78.2 ppm.

To enable peak assignments for all compositions and to test whether there is random mixing of the Ca and Mg cations on the dodecahedral sites, we have calculated the probabilities for the 15 possible cation configurations assuming a model of complete randomness (Table 4). These theoretical values can be compared with the fitted peak intensities in the experimentally measured spectra. To do so the spectra of pyrope and grossular were first fitted without constraints to obtain information about their characteristic peak shapes. For the single resonance spectrum of pyrope, a peak shape of 0.70 (where 1.0 = 100% Lorentzian and 0.0 = 100% Gaussian) with 0.44 ppm FWHM and for grossular a value of 0.54 with a FWHM of 0.47 ppm were obtained. The spectra of $Py_{90}Gr_{10}$ and $Py_{75}Gr_{25}$ were fitted next, again without constraints, where the peak shapes were expected to lie between 0.70 and 0.54. However, surprisingly, the fitted peak shapes were highly variable and ranged from completely Lorentzian to completely Gaussian (Table 5). Moreover, the same resonance did not maintain its peak shape with changing composition. For example, the strong resonance at -72.3 ppm (MgMg-MgMgMgMg) has in pyrope a measured peak shape value of 0.70, but in $Py_{90}Gr_{10}$ it has a value of 0.31 and in $Py_{75}Gr_{25}$ a value of 0.65. The resonance at -73.4 ppm (MgMg-MgMgMgCa) has a peak shape value of 0.61 in $Py_{90}Gr_{10}$ and a value of 0.00 (i.e., pure Gaussian) in $Py_{75}Gr_{25}$. There was also no systematic variation found in the change of the peak shapes.

Because peaks are strongly overlapping in the spectra of the other solid solutions with $X_{Ca} \geq 0.25$, the peak

TABLE 5. Fitting results for $Py_{90}Gr_{10}$ and $Py_{75}Gr_{25}$

$Py_{90}Gr_{10}$				$Py_{75}Gr_{25}$			
Peak position (ppm)	Peak shape*	FWHM (ppm)	Area (%)	Peak position (ppm)	Peak shape*	FWHM (ppm)	Area (%)
Without imposed constraints							
-72.3	0.31	0.54	50.7	-72.3	0.65	0.61	27.7
-73.5	0.61	0.61	25.8	-73.4	0.00	0.62	17.7
-74.6	0.00	0.55	3.4	-74.4	1.00	0.61	14.3
-75.5	0.13	0.61	11.2	-75.5	0.17	0.69	15.2
-76.7	1.00	0.69	8.7	-76.7	0.00	0.82	14.9
				-77.8	0.57	0.87	10.2
With constrained peak shapes							
-72.3	0.28	0.54	53.1	-72.3	0.58	0.62	26.2
-73.5	0.28	0.61	23.8	-73.4	0.58	0.63	21.9
-74.6	0.28	0.54	4.1	-74.4	0.58	0.55	8.6
-75.5	0.28	0.61	12.8	-75.5	0.58	0.67	16.4
-76.7	0.28	0.64	6.1	-76.7	0.58	0.72	15.2
				-77.8	0.58	0.87	8.6
				-78.8	0.58	0.88	2.7

* The value 0.0 = 100% Gaussian, 1.0 = 100% Lorentzian.

shapes of the individual resonances could not be uniquely defined and therefore had to be constrained during fitting. Inasmuch as the major goal of this work was to determine whether there is complete random mixing of the Mg and Ca cations or whether any short-range order is present, a fitting procedure was established to generate relative peak intensities that would match those arising solely from random mixing. In this manner, all resonances of a given spectrum were fixed to have the same peak shape as that of the most intense resonance. This fitting procedure was then used on all samples and first with those compositions nearest to the end-members pyrope and grossular (i.e., $Py_{90}Gr_{10}$ and $Py_{0.5}Gr_{99.5}$). Next, the spectrum with the higher pyrope or grossular content, respectively, was fitted (i.e., toward the center of the binary). Chemical shift values for resonances obtained in the preceding spectrum were used as a constrained input parameter for the fit of the next composition. The peak positions were constrained such that the difference between the chemical shifts of two neighboring resonances was kept the same. The FWHM values were, instead, varied slightly, always trying to keep them as similar as possible to the parameters obtained from the previously fitted spectrum. By varying the different parameters, we compared the fitted intensities to those probabilities calculated for a model based on a random distribution. Using this constrained procedure, the relative fitted intensities are probably not strictly quantitative, but deviations from complete random mixing can indeed be tested. In Table 5 the fitted relative intensities for $Py_{90}Gr_{10}$ and $Py_{75}Gr_{25}$ are given as examples when peak shapes were constrained. The intensities differ between 1 and 5% compared to intensities obtained in fits with no imposed constraints (Table 5). It was observed that the relative peak intensities remain nearly constant in both fitting models. Because of the strong overlapping of peaks in the spectra with $X_{Ca} \geq 0.25$, we believe the error in the estimated intensities is slightly greater, around 5%.

TABLE 6. Statistical probabilities for $\text{Py}_{90}\text{Gr}_{10}$ (i.e., $X_{\text{Ca}} = 0.1$) calculated after Table 4

Second shell	First shell		
	MgMg	MgCa	CaCa
MgMgMgMg	53.14*	11.81	0.66
MgMgMgCa	23.62	5.25	0.29
MgMgCaCa	3.94	0.87	0.05
MgCaCaCa	0.29	0.06	0.00
CaCaCaCa	0.01	0.00	0.00
Sum	81.00	18.00	1.00

* Data were multiplied by 100 to obtain values in percent.

In the case of $\text{Py}_{90}\text{Gr}_{10}$, five of the 15 possible cation configurations have probabilities $>1\%$ for random mixing (Table 6) and should therefore be experimentally detectable. Peak assignments for the configurations MgMg-MgMgMgMg and MgMg-MgMgMgCa have already been determined as discussed above. The configuration MgMg-MgMgMgMg has the greatest statistical probability of 53.1%, and MgMg-MgMgMgCa gives the second most probable configuration at 23.6%; both are consistent with their experimentally measured intensities. The configuration with the third highest statistical probability is MgCa-MgMgMgMg, calculated as 11.8%, and this matches the resonance at -75.5 ppm. Probabilities for MgMg-MgMgCaCa and MgCa-MgMgMgCa are calculated to be 3.94 and 5.25%, respectively. The resonance corresponding to MgCa-MgMgMgCa must have a greater chemical shift compared to the resonance corresponding to the configuration MgCa-MgMgMgMg because of the additional Ca cation in the second shell. Thus the resonance at -76.7 ppm is readily assigned to the latter and the resonance at -73.5 ppm to the former.

The resonances at -77.8 and -78.8 ppm in $\text{Py}_{85}\text{Gr}_{15}$ and $\text{Py}_{75}\text{Gr}_{25}$ can be assigned to the configurations MgCa-MgMgCaCa and MgCa-MgCaCaCa, respectively. The resonances with only Mg cations in the first shell differ by about 1.1 ppm. Assuming a constant shift of 1.1 ppm for the substitution for each additional Ca for Mg in the

second shell, the statistically unlikely resonances corresponding to MgMg-MgCaCaCa and MgMg-CaCaCaCa should have chemical shifts around -75.6 and -76.7 ppm and should be hidden by the resonances corresponding to MgCa-MgMgMgMg and MgCa-MgMgMgCa. For this pyrope-rich composition the statistical probabilities for MgMg-MgCaCaCa and MgMg-CaCaCaCa are at least six times less than configurations MgCa-MgMgMgMg and MgCa-MgMgMgCa. The probability of MgMg-MgCaCaCa lies, for the compositions $\text{Py}_{60}\text{Gr}_{40}$, $\text{Py}_{50}\text{Gr}_{50}$, and $\text{Py}_{40}\text{Gr}_{60}$, between 5 and 6% and has about the same probability as configuration MgCa-MgMgMgMg; hence their probabilities were summed together. The same resonance assignments were obtained for the three most grossular-rich solid solutions using model peak intensities as by the qualitative crystal chemical considerations. Peak assignments for the 13 observed resonances are summarized in Table 7. The results of the comparison between model and experimental intensities for spectra of the nine different solid solutions are given in Table 8.

The resonances with only Ca cations in the first shell differ by about 0.7 ppm, whereas those with only Mg cations differ by 1.1 ppm. Therefore resonances resulting from the configurations CaCa-XXXX are more strongly overlapping, whereas those of MgMg-XXXX are well resolved. The better resolution in the latter is best explained by the lesser degree of shielding afforded by the smaller Mg cations compared to the larger Ca ones.

Order-disorder

In the case of compositions $\text{Py}_{90}\text{Gr}_{10}$, $\text{Py}_{10}\text{Gr}_{90}$, and $\text{Py}_{05}\text{Gr}_{95}$ there is good agreement between a model with complete Ca and Mg cation disorder and the measured intensities. For example, in $\text{Py}_{90}\text{Gr}_{10}$ the difference between the calculated probabilities and the observed intensities is $<1\%$, for $\text{Py}_{10}\text{Gr}_{90}$ the difference is $<2\%$, and for $\text{Py}_{05}\text{Gr}_{95}$ it is $<5\%$. Since peak overlapping in grossular-rich garnets is strong, we do not consider this latter deviation to be significant and conclude that a random

TABLE 7. Peak assignments for pyrope-grossular garnets*

First shell	Second shell	Pyrope	$\text{Py}_{90}\text{Gr}_{10}$	$\text{Py}_{85}\text{Gr}_{15}$	$\text{Py}_{75}\text{Gr}_{25}$	$\text{Py}_{60}\text{Gr}_{40}$	$\text{Py}_{50}\text{Gr}_{50}$	$\text{Py}_{40}\text{Gr}_{60}$	$\text{Py}_{25}\text{Gr}_{75}$	$\text{Py}_{10}\text{Gr}_{90}$	$\text{Py}_{05}\text{Gr}_{95}$	Grossular
MgMg-	MgMgMgMg	-72.0	-72.3	-72.2	-72.3	-72.5	-72.5					
	MgMgMgCa		-73.4	-73.3	-73.4	-73.6	-73.6	-73.7				
	MgMgCaCa		-74.6	-74.5	-74.4	-74.6	-74.7	-74.7				
	MgCaCaCa				-75.5	-75.7	-75.8	-75.8				
	CaCaCaCa				-75.5	-75.7	-75.8	-76.6				
MgCa-	MgMgMgMg		-75.5	-75.4	-75.5	-75.7	-75.8	-75.8				
	MgMgMgCa		-76.7	-76.6	-76.7	-77.0	-77.1	-77.3	-77.4			
	MgMgCaCa			-77.7	-77.8	-78.1	-78.2	-78.3	-78.2			
	MgCaCaCa				-78.8	-79.1	-79.1	-79.1	-79.1	-79.3		
	CaCaCaCa					-79.9	-79.9	-79.8	-79.9	-80.1	-80.1	
CaCa-	MgMgMgMg					-81.1	-80.9	-81.1				
	MgMgMgCa					-82.1	-81.5	-81.7	-81.3			
	MgMgCaCa						-82.3	-82.6	-82.1	-82.5		
	MgCaCaCa						-83.0	-83.2	-82.8	-83.1	-83.1	
	CaCaCaCa						-83.5	-83.7	-83.5	-83.8	-83.8	-83.8

* Peak position in parts per million.

TABLE 8. Relative intensities obtained from constrained fits compared to the calculated random probabilities in the ^{29}Si NMR spectra of pyrope-grossular solid solutions

First shell	Second shell	Peak position (ppm)	FWHM (ppm)	I_{obs} fitted areas (%)	I_{calc} calculated prob. (%)	$I_{\text{obs}} - I_{\text{calc}}$ intensity diff. (%)
Py₉₀Gr₁₀						
MgMg-	MgMgMgMg	-72.3	0.54	53.2	53.1*	0.1
	MgMgMgCa	-73.5	0.60	23.9	23.6	0.3
	MgMgCaCa	-74.6	0.54	4.1	3.9	0.2
MgCa-	MgMgMgMg	-75.5	0.61	12.8	11.8	1.0
	MgMgMgCa	-76.7	0.64	6.1	5.2	0.9
Py₈₅Gr₁₅						
MgMg-	MgMgMgMg	-72.2	0.76	44.2	37.7	6.5
	MgMgMgCa	-73.3	0.81	25.8	26.6	-0.8
	MgMgCaCa	-74.5	0.69	5.2	7.1	-1.9
MgCa-	MgMgMgMg	-75.4	0.77	14.2	13.3	0.9
	MgMgMgCa	-76.6	0.86	8.5	9.4	-0.9
	MgMgCaCa	-74.7	0.61	2.0	2.5	-0.5
Py₇₅Gr₂₅						
MgMg-	MgMgMgMg	-72.3	0.62	26.5	17.8	8.7
	MgMgMgCa	-73.4	0.63	21.9	23.7	-1.8
	MgMgCaCa	-74.4	0.55	8.6	11.9	-3.3
MgCa-	MgMgMgMg	-75.5**	0.67	16.5	11.9; 14.7	4.6; 1.8
	MgMgMgCa	-76.7	0.72	15.2	15.8	-0.6
	MgMgCaCa	-77.8	0.87	8.6	7.9	0.7
	MgCaCaCa	-78.8	0.88	2.7	1.8	0.9
Py₆₀Gr₄₀						
MgMg-	MgMgMgMg	-72.5	0.66	5.0	4.7	0.3
	MgMgMgCa	-73.6	0.71	11.1	12.4	-1.3
	MgMgCaCa	-74.6	0.9	11.2	12.4	-1.2
MgCa-	MgMgMgMg	-75.7**	0.902	12.8	6.2; 12.7	6.6; 0.1
	MgMgMgCa	-77.0	0.870	18.5	16.6	1.9
	MgMgCaCa	-78.1	0.87	18.7	16.6	2.1
	MgCaCaCa	-79.1	0.77	10.1	7.4	2.7
CaCa-	CaCaCaCa	-79.9	0.71	5.4	1.2	4.2
	MgMgMgMg	-81.1	0.88	4.6	2.0	2.6
	MgMgMgCa	-82.1	0.810	2.7	5.5	-2.8
Py₅₀Gr₅₀						
MgMg-	MgMgMgMg	-72.5	0.52	1.6	1.6	0.0
	MgMgMgCa	-73.6	0.66	5.4	6.3	-0.9
	MgMgCaCa	-74.7	0.89	8.7	9.4	-0.7
MgCa-	MgMgMgMg	-75.8**	0.96	10.1	3.1; 10.9	7.0; -0.8
	MgMgMgCa	-77.1	0.67	10.9	12.5	-1.6
	MgMgCaCa	-78.2	1.14	24.2	18.8	5.4
	MgCaCaCa	-79.1	1.04	17.9	12.5	5.4
CaCa-	CaCaCaCa	-79.9	0.75	5.7	3.1	2.6
	MgMgMgMg	-80.9	0.64	2.7	1.6	1.1
	MgMgMgCa	-81.5	0.64	4.7	6.3	-1.6
	MgMgCaCa	-82.3	0.690	4.9	9.4	-4.5
	MgCaCaCa	-83.0	0.59	2.4	6.3	-3.9
	CaCaCaCa	-83.5	0.55	0.9	1.6	-0.7
Py₄₀Gr₆₀						
MgMg-	MgMgMgCa	-73.7	0.71	3.4	2.5	0.9
	MgMgCaCa	-74.7	0.73	4.2	5.5	-1.3
	CaCaCaCa	-76.6	0.8	1.9	2.0	-0.1
MgCa-	MgMgMgMg	-75.8**	0.93	7.0	1.2; 6.8	5.8; 0.2
	MgMgMgCa	-77.3	0.87	7.8	7.4	0.4
	MgMgCaCa	-78.3	0.89	16.8	16.6	0.2
	MgCaCaCa	-79.1	0.85	17.6	16.6	1.0
CaCa-	CaCaCaCa	-79.8	0.87	13.3	6.2	7.1
	MgMgMgMg	-81.1	0.82	3.2	0.9	2.3
	MgMgMgCa	-81.7	0.79	8.1	5.5	2.6
	MgMgCaCa	-82.6	0.79	9.3	12.4	-3.1
	MgCaCaCa	-83.2	0.730	6.0	12.4	-6.4
	CaCaCaCa	-83.7	0.69	1.3	4.7	-3.4
Py₂₅Gr₇₅						
MgCa-	MgMgMgCa	-77.4	0.83	3.0	1.8	1.2
	MgMgCaCa	-78.2	0.8	7.9	7.9	0.0
	MgCaCaCa	-79.1	0.83	15.9	15.8	0.1
CaCa-	CaCaCaCa	-79.9	0.8	18.8	11.9	6.9
	MgMgMgCa	-81.3	0.84	5.2	2.6	2.6
	MgMgCaCa	-82.1	0.78	10.4	11.9	-1.9

TABLE 8.—Continued

First shell	Second shell	Peak position (ppm)	FWHM (ppm)	I_{obs} fitted areas (%)	I_{calc} calculated prob. (%)	$I_{\text{obs}} - I_{\text{calc}}$ intensity diff. (%)
	MgCaCaCa	-82.8	0.71	16.0	23.7	-7.7
	CaCaCaCa	-83.5	0.77	22.8	17.8	5.0
			Py₁₀Gr₉₀			
MgCa-	MgCaCaCa	-79.3	0.97	6.2	5.3	0.9
	CaCaCaCa	-80.1	0.58	12.6	11.8	0.8
CaCa-	MgMgCaCa	-82.5	0.79	4.2	3.9	0.3
	MgCaCaCa	-83.1	0.79	25.3	23.6	1.7
	CaCaCaCa	-83.8	0.63	51.6	53.1	-1.5
			Py₉₅Gr₉₅			
MgCa-	CaCaCaCa	-80.1	0.7	6.3	7.7	-1.4
CaCa-	MgCaCaCa	-83.1	0.77	15.2	15.5	-0.3
	CaCaCaCa	-83.8	0.64	78.4	73.5	4.9

* The calculated probabilities do not necessarily sum to 100%, because only those configurations that have been fitted have been considered.

** The first probability corresponds to MgCa-MgMgMgMg and the second, to the right of the semicolon, to the sum of the configurations MgCa-MgMgMgMg and MgMg-MgCaCaCaCa.

distribution of Ca and Mg exists for compositions $0.9 \leq X_{\text{Mg}} \leq 0.1$.

The observed intensity of the MgMg-MgMgMgMg configuration in the spectrum of Py₈₅Gr₁₅ is 6.5% greater than the calculated probability for random disorder (Table 8). The same observation is true for Py₇₅Gr₂₅, where the intensity is 8.7% larger than the calculated random model, and moreover, the configuration with the highest statistical probability is MgMg-MgMgMgCa, whereas in the measured spectrum the peak corresponding to this configuration is only the second most intense peak. This deviation from a random mixing model is too great to be explained by errors in the fitting procedure. A similar deviation is observed in the more grossular-rich garnet Py₂₅Gr₇₅. Here the most probable random configuration is CaCa-MgCaCaCa, whereas the resonance with the greatest observed intensity lies at -83.8 ppm, corresponding to the CaCa-CaCaCaCa configuration. Moreover, the intensity of the resonance at -83.1, corresponding to CaCa-MgCaCaCa, is 7.7% less than the calculated probability, and the intensity of the peak corresponding to MgCa-CaCaCaCa is 6.9% higher than that expected for a completely random distribution. Since the configuration CaCa-CaCaCaCa is preferred in the experimental spectrum over other Ca-containing configurations, one has to compensate for the additional Ca to maintain bulk composition. This seems to be done by a lesser occupation of the configurations CaCa-MgCaCaCa and CaCa-MgMgCaCa combined with a greater occupation of the configuration CaMg-CaCaCaCa. An analogous situation is observed for Py₈₅Gr₁₅ and Py₇₅Gr₂₅. The preference for the configuration MgMg-MgMgMgMg is compensated by lesser observed intensity in MgMg-MgMgMgCa and more observed intensity in MgCa-MgMgMgMg compared to a random model. The deviations are much smaller than in Py₂₅Gr₇₅, <2%, but they follow the same pattern.

The peak fits of the Py₆₀Gr₄₀, Py₅₀Gr₅₀, and Py₄₀Gr₆₀ spectra have larger errors because of their greater peak overlapping. Nevertheless, there are indications that de-

viations from random mixing behavior can be discerned. In all three compositions, if one considers the peak intensity ratios rather than their absolute values, one observes a preference for those configurations with one Mg and one Ca cation in the first shell. In Py₆₀Gr₄₀, for example, the intensity ratio of MgCa-MgMgMgCa to MgMg-MgMgMgCa in the random model should be 16.6%/12.4% = 1.34 (Table 8), but this value cannot be approached better than 18.6%/11.2% = 1.67 by changing the fit variables. In Py₄₀Gr₆₀ a similar relationship of MgCa-MgCaCaCa to CaCa-MgCaCaCa (16.6%/12.4%) is best approximated by 16.8%/9.3% = 1.8 and 17.6%/6.0% = 2.9. In Py₅₀Gr₅₀ resonances corresponding to MgCa-XXXX have greater observed intensities than their calculated probabilities, whereas MgMg-XXXX and CaCa-XXXX resonances have smaller intensities than those calculated. The peak intensities should be symmetric around MgCa-MgMgCaCa in a totally random model, and the configurations MgCa-MgCaCaCa and MgCa-MgMgMgCa should have the same intensities, yet the latter has 7% less observed intensity.

An important question arising from these measurements is whether the garnets were in thermodynamic equilibrium at their respective *P-T* synthesis conditions. The ²⁹Si MAS NMR spectra of two different Py₉₀Gr₁₀ samples synthesized at 1250 and 1450 °C, respectively, show no difference in their relative peak intensities (Geiger et al., 1990b). Hence, the simplest conclusion for this composition is that mixing of Ca and Mg cations on the dodecahedral site is independent of *T* in this region and that, once again, there is total random cation disorder. An indication of possible equilibrium is also found in those compositions in which deviations from totally random mixing occur, because the fitted intensities deviate from the random statistical probabilities in a systematic way. For example, in the spectra of Py₇₅Gr₂₅ and Py₂₅Gr₇₅, where the deviations are clearest, the configurations corresponding to MgMg-MgMgMgMg or CaCa-CaCaCaCa are strongly preferred over configurations MgMg-Mg-

MgMgCa and CaCa-MgCaCaCa, respectively. As the binary pyrope-grossular is probably characterized by a solvus (Haselton and Newton, 1980), the presence of short-range order favoring pyrope- and grossular-like domains in these two solid solutions may be interpreted as cluster building as a precursor to unmixing. This relation between ordering and unmixing in solid solutions is likely in several silicate solid solutions (Carpenter, 1985). Therefore, we believe these garnets do not depart greatly from chemical equilibrium.

The equivalent site model advanced by Newton and Wood (1980) to explain the asymmetric ΔV_{mix} observed in several binary silicate solid solutions may not hold for pyrope-grossular garnets. The NMR spectra show no overt evidence for short-range order in the most pyrope-rich compositions with $X_{\text{Mg}} \geq 0.9$, where Mg-Ca ordering should be present. Short-range order is measurable in composition $\text{Py}_{85}\text{Gr}_{15}$, however. Unfortunately, the model is difficult to test quantitatively, because those configurations having two Ca atoms in edge-sharing dodecahedra of the second shell, for example, are statistically unlikely and experimentally difficult to observe. Further microscopic properties need to be clarified before the volumes of mixing in garnet solid solutions can be understood.

Phase equilibrium experiments involving garnet in equilibrium with orthopyroxene and clinopyroxene in the CMAS system show that the garnet composition $\text{Py}_{86}\text{Gr}_{14}$ remains nearly constant over a wide range of P - T conditions (Perkins and Newton, 1980). In addition, thermodynamic calculations of the slope and position of the reaction boundary for clinopyroxene + orthopyroxene + spinel = garnet + forsterite require garnet to have near-zero or negative excess entropies at compositions close to $\text{Py}_{85}\text{Gr}_{15}$ to match the experimentally determined reaction curve (Wood and Holloway, 1984). The measurable short-range order found in $\text{Py}_{85}\text{Gr}_{15}$ offers a possible explanation for the former experimental observation and is consistent with the thermodynamic conclusions proposed in the latter theoretical study.

The presence of short-range order, on the other hand, in pyrope-grossular garnets with compositions between $0.15 \leq X_{\text{Ca}} \leq 0.75$ requires the configurational entropy of mixing to be smaller than that based on a completely random model. The synthesis conditions used here were mainly above 1100 °C and the degree of order should increase with decreasing temperature. This could have potential significance for thermodynamic mixing models pertaining to many natural garnets that equilibrate between 500 and 900 °C. Further work is needed, especially on solid solutions equilibrated at different temperatures, to formulate a model that can explain the deviations from complete random disorder.

ACKNOWLEDGMENTS

This work has been supported by the Deutsche Forschungsgemeinschaft, grant number Ge 649/2-1, as part of a priority program concerning

element partitioning in rock-forming silicates. A.S. gratefully acknowledges support by the Deutsche Forschungsgemeinschaft and the Fonds der chemischen Industrie. We thank J. Kümmerlen for his help with the fitting routines, W. Preetz for use of the IR spectrometer, and U. Kornelissen for technical assistance.

REFERENCES CITED

- Armbruster, T., Geiger, C.A., and Lager, G.A. (1992) Single-crystal X-ray structure study of synthetic pyrope almandine garnets at 100 and 293 K. *American Mineralogist*, 77, 512–521.
- Carpenter, M.A. (1985) Order-disorder transformations in mineral solid solutions. In *Mineralogical Society of America Reviews in Mineralogy*, 14, 187–223.
- Delany, J.M. (1981) A spectral and thermodynamic investigation of synthetic pyrope-grossular garnets, 201 p. Ph.D. thesis, University of California, Los Angeles, California.
- Dempsey, M.J. (1980) Evidence for structural changes in garnet caused by calcium substitution. *Contributions to Mineralogy and Petrology*, 71, 281–282.
- Engelhardt, G., and Michel, D. (1987) High-resolution solid-state NMR of silicates and zeolites, 485 p. Wiley, New York.
- Ganguly, J., Cheng, W., and O'Neill, H.St.C. (1993) Syntheses, volume, and structural changes of garnets in the pyrope-grossular join: Implications for stability and mixing properties. *American Mineralogist*, 78, 583–593.
- Geiger, C.A., Winkler, B., and Langer, K. (1989) Infrared spectra of synthetic almandine-grossular and almandine-pyrope garnet solid solutions: Evidence for equivalent site behaviour. *Mineralogical Magazine*, 53, 231–237.
- Geiger, C.A., Merwin, L., and Sebald, A. (1990a) Ordering studies in grossular and pyrope garnets using ^{29}Si NMR and ^{57}Fe Mössbauer spectroscopy (abs.), p. 11–12. Third International Symposium of Experimental Mineralogy, Petrology and Geochemistry, Edinburgh, U.K.
- (1990b) Pyrope-grossular garnets: Synthesis and ^{29}Si MAS NMR spectroscopy (abs.), p. 1666. American Geophysical Union Fall Meeting, San Francisco, California.
- (1992) Structural investigation of pyrope garnet using temperature-dependent FTIR and ^{29}Si and ^{27}Al MAS NMR spectroscopy. *American Mineralogist*, 77, 713–717.
- Haselton, H.T., and Newton, R.C. (1980) Thermodynamics of pyrope-grossular garnets and their stabilities at high temperatures and pressures. *Journal of Geophysical Research*, 85, 6973–6982.
- Haselton, H.T., and Westrum, E.J. (1980) Low-temperature heat capacities of synthetic pyrope, grossular, and pyrope60-grossular40. *Geochimica et Cosmochimica Acta*, 44, 701–709.
- Hofmeister, A.M., and Chopelas, A. (1991) Vibrational spectroscopy of end-member silicate garnets. *Physics and Chemistry of Minerals*, 17, 503–526.
- McMillan, P., Akaogi, M., Ohtani, E., Williams, Q., Niemann, R., and Sato, R. (1989) Cation disorder in garnets along the $\text{Mg}_3\text{Al}_2\text{Si}_3\text{O}_{12}$ - $\text{Mg}_2\text{Si}_4\text{O}_{12}$ join: An infrared, Raman and NMR study. *Physics and Chemistry of Minerals*, 16, 428–435.
- Menzer, G. (1928) Die Kristallstruktur der Granate. *Zeitschrift für Kristallographie*, 69, 300–396.
- Merwin, L.H., Sebald, A., Espidel, J.E., and Harris, R.K. (1989) An airtight inexpensive, easy to use MAS rotor insert. *Journal of Magnetic Resonance*, 84, 367–371.
- Moore, R.K., White, W.B., and Long, T.V. (1971) Vibrational spectra of the common silicates: I. The garnets. *American Mineralogist*, 56, 54–71.
- Newton, R.C., and Wood, B.J. (1980) Volume behavior of silicate solid solutions. *American Mineralogist*, 65, 733–745.
- Newton, R.C., Charlu, T.V., and Kleppa, O.J. (1977) Thermochemistry of high pressure garnets and clinopyroxenes in the system $\text{CaO-MgO-Al}_2\text{O}_3\text{-SiO}_2$. *Geochimica et Cosmochimica Acta*, 41, 369–377.
- Novak, G.A., and Gibbs, G.V. (1971) The crystal chemistry of the silicate garnets. *American Mineralogist*, 56, 791–825.
- Perkins, D., and Newton, R.C. (1980) The compositions of coexisting

- pyroxenes and garnet in the system CaO-MgO-Al₂O₃-SiO₂ at 900°-1,100° C and high pressures. *Contributions to Mineralogy and Petrology*, 75, 291-300.
- Renner, B., and Lehmann, G. (1986) Correlation of angular and bond length distortions in TO₄ units in crystals. *Zeitschrift für Kristallographie*, 175, 43-59.
- Tarte, P. (1962) Etudes experimentale et interpretation du spectre infrarouge des silicates et des germanates. Application a des problems structuraux relatifs a l'etat solide. *Mémoires de l'Académie Royale de Belgique*, 35, 103-119.
- Wood, B.J., and Holloway, J.R. (1984) A thermodynamic model for subsolidus equilibria in the system CaO-MgO-Al₂O₃-SiO₂. *Geochimica et Cosmochimica Acta*, 48, 159-176.

MANUSCRIPT RECEIVED OCTOBER 21, 1994

MANUSCRIPT ACCEPTED MARCH 21, 1995